JOC Article

Lack of Visible Chromophore Development in the Pulse Radiolysis Oxidation of 5,6-Dihydroxyindole-2-carboxylic Acid Oligomers: DFT Investigation and Implications for Eumelanin Absorption Properties

Alessandro Pezzella,[†] Lucia Panzella,[†] Orlando Crescenzi,[‡] Alessandra Napolitano,[†] Suppiah Navaratnam,[§,||] Ruth Edge,[§,¶,⊥] Edward J. Land,[¶] Vincenzo Barone,*[,#] and Marco d'Ischia*[,†]

Department of Organic Chemistry and Biochemistry and "Paolo Corradini" Department of Chemistry, University of Naples Federico II, Via Cinthia 4, I-80126 Naples, Italy, STFC Daresbury Laboratory, Daresbury, WA4 4AD, United Kingdom, BioScience Research Institute, Peel Building, University of Salford, Salford M5 4WT, United Kingdom, Chemistry Section, School of Physical and Geographical Sciences, Keele University, Staffs ST5 5BG, United Kingdom, School of Chemistry, University of Manchester, Oxford Road, Manchester, M22 9PL, United Kingdom, and Scuola Normale Superiore di Pisa, Piazza dei Cavalieri 7, I-56125 Pisa, Italy

vincenzo.barone@sns.it; dischia@unina.it

Received February 4, 2009

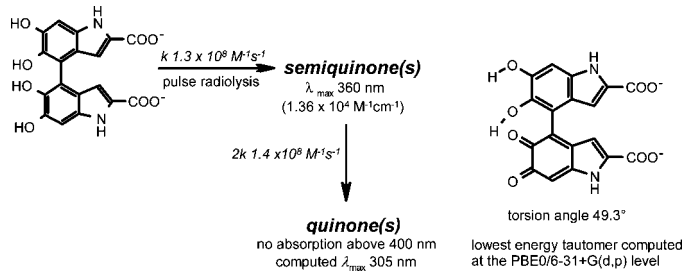

The structural factors underlying the peculiar optical properties and visible chromophore of eumelanin biopolymers are largely uncharted. It is known that synthetic eumelanins from 5,6-dihydroxyindole are black and display a featureless UV−visible absorption spectrum, whereas those from 5,6-dihydroxyindole-2-carboxylic acid (**1**) are lighter in color and exhibit a distinct band around 310 nm, but the origin of this difference has never been addressed in detail. Recently, we showed that 5,6-dihydroxyindole dimers generate on pulse radiolysis oxidation strongly absorbing transients with intense maxima in the 500−600 nm region, which have been attributed to planar extended quinone methide species. We now report the unexpectedly different behavior of three oligomers from **1**, namely, the 4,4′-biindolyl **2**, the 4,7′-biindolyl **3**, and the 4,7′:4′,7″-terindolyl **4**. Pulse radiolysis oxidation of **2**−**4** led initially to semiquinone intermediates exhibiting similar absorption maxima at 360−380 nm. Semiquinone absorption decay followed second-order kinetics ($2k = 1.4 \times 10^8$, 3.2×10^8, and 1.4×10^8 M^{-1} s^{-1} for **2**, **3**, and **4**, respectively) but did not lead to significant chromophore development in the visible region. Similar absorption traces were obtained from monomer **1**. DFT calculations predicted 5,6-dihydroxyindolyl-5,6-indolequinone structures with significant dihedral twists across the interunit single bonds for the most stable two-electron oxidation products of **2** and **3**. The computed absorption spectra consistently featured strong bands around 310 nm but little or no absorption in the visible region. It is suggested that the effective conjugation length in oligomeric/polymeric eumelanin components from **1** may be controlled by hindered rotation around inter-ring bonds preventing planarization of the continuous array of indole units. This may provide an explanation for the difference in the absorption properties of polymers from the two key eumelanin monomers.

Introduction

Eumelanins, the characteristic black biopolymers found in human skin, hair, and eyes,[1] are produced by oxidative polymerization of 5,6-dihydroxyindole-2-carboxylic acid (**1**) and the parent 5,6-dihydroxyindole, two highly oxidizable, catechol-containing indoles derived biosynthetically from tyrosine. Apart from their central role in pigmentation and related disorders, such as melanoma, eumelanins have intrigued generations of chemists and biophysicists because of their unique physicochemical properties,[2] including a broad absorbance profile throughout the entire UV−visible region, strong nonradiative

[†] Department of Organic Chemistry and Biochemistry, University of Naples Federico II.
[‡] "Paolo Corradini" Department of Chemistry, University of Naples Federico II.
[§] STFC Daresbury Laboratory.
[||] University of Salford.
[¶] Keele University.
[⊥] University of Manchester.
[#] Scuola Normale Superiore di Pisa.

10.1021/jo900250v CCC: $40.75 © 2009 American Chemical Society
Published on Web 04/22/2009

relaxation of photoexcited electronic states,[3] a persistent EPR signal,[4] and semiconductor-like behavior.[5] These properties are most relevant to the functional significance of eumelanins, for example, in photoprotection,[6] and have recently spurred investigation of related 5,6-dihydroxyindole-based polymers as soft, biocompatible functional materials for molecular electronics.[7]

Despite extensive efforts,[1,2] the fundamental structure and optoelectronic properties of eumelanins have remained little understood because of the intractable nature of these polymers, including a marked insolubility, an extremely high molecular heterogeneity, an ill-defined electronic state (believed to encompass mixtures of species at the catechol, semiquinone, or quinone state), and an amorphous solid character. Most of the current knowledge of eumelanin structure has been derived from direct investigation of natural[8] and synthetic[9,10] pigments and from systematic studies of the oxidative polymerization of 5,6-dihydroxyindoles and their oligomers as a model process mimicking polymer buildup.[11,12] A crucial, still pending issue from the above studies concerns the markedly different properties of synthetic eumelanins from the two monomer precursors; whereas 5,6-dihydroxyindole-derived polymers are black and exhibit a monotonic, featureless absorption spectrum, those from **1** are lighter in color and display a detectable inflection around 310 nm. The relevance of this point to natural biopolymers is illustrated by the fact that eumelanin from *Sepia*, which contains a large proportion of units from **1**, features a distinct shoulder above 300 nm.[8a,13]

Studies toward this issue are notoriously difficult because of the exceptional instability of 5,6-indolequinones and related quinonoid species generated during the oxidative polymerization process, which has so far prevented a detailed understanding of their absorption properties. By using an integrated chemical, pulse radiolysis, and quantum chemical approach, it has recently been possible to gain an insight into the short-lived two-electron oxidation products of three 5,6-dihydroxyindole dimers.[14] These species exhibited intense absorption bands around 500−570 nm and were identified as almost planar extended quinone methide structures with an inter-ring double bond. Interestingly, they seemed to fit well a previously suggested "stacked-oligomer" model for eumelanin structure, envisaging π-stacking interactions between planar oligomeric scaffolds to form the fundamental nanoaggregates.[15]

Oxidation of **1** leads to a number of oligomeric products,[16−18] including the 4,4′- and 4,7′-biindolyls **2** and **3** and the terindolyl **4**. As a noticeable feature, these oligomers exhibit atropisomerism[18] due to steric constraints around the inter-ring single bond and the negatively charged carboxylate functions contributing to maintain significant twist angles. The consequences of hindered rotation around inter-ring bonds on the structure and absorption properties of oxidized oligomers/polymers of **1** appear to have escaped the attention of previous investigators and have remained largely unknown.[13,19,20]

In this paper, we report the results of a pulse radiolysis and DFT investigation of the short-lived oxidation products of oligomers **2**−**4** in comparison to **1**. Specific aim of the study was to gain a comparative insight into the absorption properties of the oxidized transient species in the series from monomer **1** to trimer **4** to assess the influence of molecular size and hindered rotation on visible chromophore development.

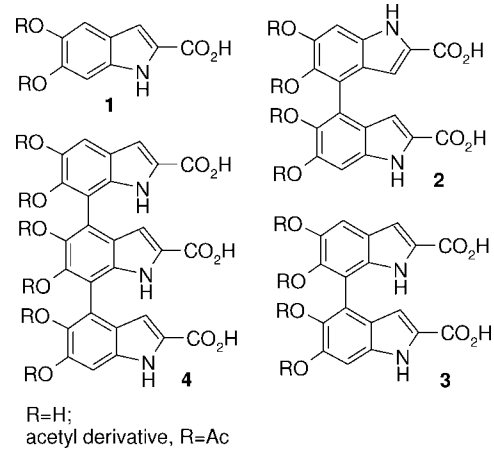

Results and Discussion

Pulse Radiolysis: Pulse radiolysis was carried out as described previously.[14,21] Generation of the oxidizing species $Br_2^{-\bullet}$ was achieved by irradiating N_2O-saturated solutions of 0.5 M KBr. Under such conditions, $Br_2^{-\bullet}$ radicals are formed within 0.1 μs after the radiation pulse according to the following equations:

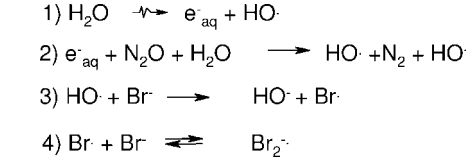

In preliminary experiments, diacetyl **1** (0.15 mM) was deacetylated and subjected to pulse radiolysis, and the results were compared with those obtained using authentic **1** at the same concentration. In both cases, a labile semiquinone (**1S**) was

(1) (a) Prota, G. *Melanins and Melanogenesis*; Academic Press: San Diego, CA, 1992. (b) *The Pigmentary System: Physiology and Pathophysiology*; Nordlund, J. J., Boissy, R. E., Hearing, V. J., King, R. A., Oetting, W. S., Ortonne, J. P., Eds.; Blackwell Publishing: Malden, MA, 2006.

(2) Meredith, P.; Sarna, T. *Pigment Cell Res.* **2006**, *19*, 572–594.

(3) (a) Nighswander-Rempel, S. P.; Riesz, J.; Gilmore, J.; Bothma, J. P.; Meredith, P. *J. Phys. Chem. B* **2005**, *109*, 20629–20635. (b) Nofsinger, J. B.; Simon, J. D. *Photochem. Photobiol.* **2001**, *74*, 31–37.

(4) Seagle, B. L.; Rezai, K. A.; Gasyna, E. M.; Kobori, Y.; Rezaei, K. A.; Norris, J. R., Jr. *J. Am. Chem. Soc.* **2005**, *127*, 11220–11221.

(5) McGinness, J.; Corry, P.; Proctor, P. *Science* **1974**, *183*, 853–855.

(6) For recent perspectives on eumelanins and photoprotection, see: *Photochem. Photobiol.* **2008**, *84*.

(7) (a) Powell, B. J.; Baruah, T.; Bernstein, N.; Brake, K.; McKenzie, R. H.; Meredith, P.; Pederson, M. R. *J. Chem. Phys.* **2004**, *120*, 8608–8615. (b) de Albuquerque, J. E.; Giacomantonio, C.; White, A. G.; Meredith, P. *Eur. Biophys. J.* **2006**, *35*, 190–195. (c) Bothma, J. P.; de Boor, J.; Divakar, U.; Schwenn, P. E.; Meredith, P. *Adv. Mater.* **2008**, *20*, 3539–3542.

(8) (a) Pezzella, A.; d'Ischia, M.; Napolitano, A.; Palumbo, A.; Prota, G. *Tetrahedron* **1997**, *53*, 8281–8286. (b) Clancy, C. M. R.; Simon, J. D. *Biochemistry* **2001**, *40*, 13353–13360. (c) Liu, Y.; Simon, J. D. *Pigment Cell Res.* **2003**, *16*, 606–618. (d) Nofsinger, J. B.; Weinert, E. E.; Simon, J. D. *Biopolymers* **2002**, *61*, 302–305.

(9) (a) Napolitano, A.; Pezzella, A.; Prota, G.; Seraglia, R.; Traldi, P. *Rapid Commun. Mass Spectrom.* **1996**, *10*, 204–208. (b) Napolitano, A.; Pezzella, A.; Prota, G.; Seraglia, R.; Traldi, P. *Rapid Commun. Mass Spectrom.* **1996**, *10*, 468–472. (c) Kroesche, C.; Peter, M. G. *Tetrahedron* **1996**, *52*, 3947–3952. (d) Lorite, G. S.; Coluci, V. R.; da Silva, M. I. N.; Deziderio, S. N.; Graeff, C. F. O.; Galvao, D. S.; Cotta, M. A. *J. Appl. Phys.* **2006**, *99*, 113511/1–113511/6.

(10) (a) Ito, S.; Wakamatsu, K. In *The Pigmentary System: Physiology and Pathophysiology*; Nordlund, J. J., Boissy, R. E., Hearing, V. J., King, R. A., Oetting, W. S., Ortonne, J. P., Eds.; Blackwell Publishing: Malden, MA, 2006; pp 282−310. (b) Napolitano, A.; Pezzella, A.; Vincensi, M. R.; Prota, G. *Tetrahedron* **1995**, *51*, 5913–5920. (c) Napolitano, A.; Pezzella, A.; d'Ischia, M.; Prota, G. *Tetrahedron* **1996**, *52*, 8775–8780.

(11) d'Ischia, M.; Napolitano, A.; Pezzella, A.; Land, E. J.; Ramsden, C. A.; Riley, P. A. *Adv. Heterocycl. Chem.* **2005**, *89*, 1–63.

(12) (a) Panzella, L.; Pezzella, A.; Napolitano, A.; d'Ischia, M. *Org. Lett.* **2007**, *9*, 1411–1414. (b) Pezzella, A.; Panzella, L.; Natangelo, A.; Arzillo, M.; Napolitano, A.; d'Ischia, M. *J. Org. Chem.* **2007**, *72*, 9225–9230. (c) Hatcher, L. Q.; Simon, J. D. *Photochem. Photobiol.* **2008**, *84*, 608–612.

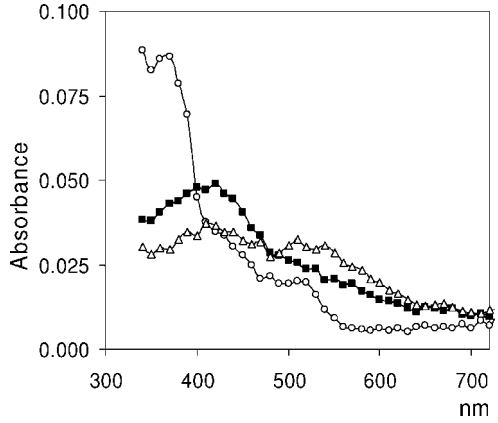

FIGURE 1. Changes in absorption at various times after pulse radiolysis of a N_2O-saturated solution of **1** (1.5×10^{-4} M) in 0.5 M KBr/7.0×10^{-2} M phosphate buffer, pH 7.0: (○) 500 μs; (■) 7 ms; (Δ) 44 ms.

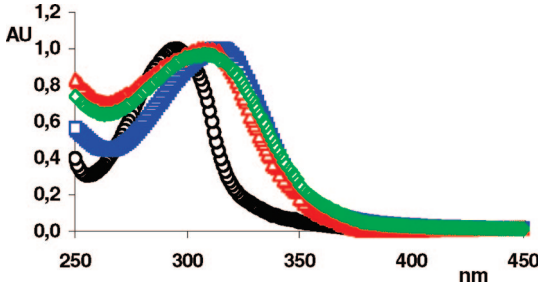

FIGURE 2. Absorption spectra of compounds **1**−**4** in 7.0×10^{-2} M phosphate buffer, pH 7.0: black trace, **1**; red trace, **2**; blue trace, **3**; green trace, **4**. Spectra are normalized at the wavelength corresponding to the absorption maximum.

detected with absorption maxima at 350 ($\varepsilon = 14\,000$) and 520 nm, which decayed with second-order kinetics ($2k = 3.5 \times 10^8$ M^{-1} s^{-1}) to give a species absorbing weakly around 430 nm (Figure 1). These results were in line with previous studies using the azide radical as the oxidizing agent.[22]

Dimers **2** and **3** and trimer **4** were likewise prepared as the acetyl derivatives and were deacetylated just prior to pulse radiolysis experiments by a recently developed procedure.[14] The steady state absorption spectra of all the deacetylated compounds are shown in Figure 2.

Figures 3 and 4 show the series of successive transient absorption spectra obtained from pulse radiolytic one-electron

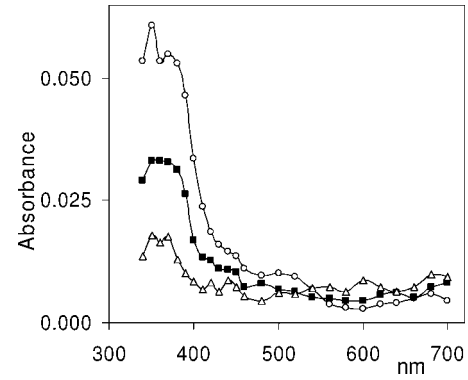

FIGURE 3. Changes in absorption at various times after pulse radiolysis of a N_2O-saturated solution of dimer **2** (1.5×10^{-4} M) in 0.5 M KBr/7.0×10^{-2} M phosphate buffer, pH 7.0: (○) 400 μs; (■) 5 ms; (Δ) 44 ms.

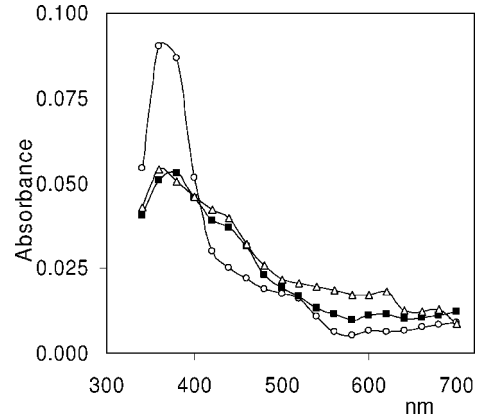

FIGURE 4. Changes in absorption at various times after pulse radiolysis of a N_2O-saturated solution of dimer **3** (1.5×10^{-4} M) in 0.5 M KBr/7.0×10^{-2} M phosphate buffer, pH 7.0: (○) 700 μs; (■) 7.6 ms; (Δ) 44 ms.

oxidation of dimers **2** and **3**, respectively. In each case, the first transient spectrum was recorded at such a time that the buildup of initial radical absorption was complete and that subsequent decay had not proceeded to any significant extent. The initial product from **2**, completely formed 400 μs after the pulse, was the semiquinone **2S**, with an intense maximum around 360 nm ($\varepsilon = 1.36 \times 10^4$ M^{-1} cm^{-1}) and a weak absorption around 500 nm, resembling semiquinone **1S**. The rate constant for the reaction of **2** with $Br_2^{-\bullet}$ was estimated to be $k = 1.3 \times 10^8$ M^{-1} s^{-1}.

Subsequent decay of the semiquinone **2S** followed second-order kinetics ($2k = 1.4 \times 10^8$ M^{-1} s^{-1}) and did not result in any significant chromophore formation in the 400−700 nm region. Data in Figure 4 indicated a similar behavior of dimer **3**. Its semiquinone (**3S**) exhibited an absorption maximum at 360 nm ($\varepsilon = 1.60 \times 10^4$ M^{-1} cm^{-1}), was produced with a formation rate constant $k = 7.7 \times 10^8$ M^{-1} s^{-1}, and decayed by second-order kinetics ($2k = 3.2 \times 10^8$ M^{-1} s^{-1}), leading within the first milliseconds to a species (or mixture of species) with a similar absorption peak at 380 nm ($\varepsilon = 11\,900$ M^{-1} cm^{-1}), a shoulder around 440 nm, and no significant absorption in the remainder of the visible region. A similar absorption trace was detectable 44 ms after the pulse.

The pulse radiolysis behavior of trimer **4** is shown in Figure 5. The semiquinone **4S** (absorption maximum around 370 nm, $\varepsilon = 1.06 \times 10^4$ M^{-1} cm^{-1}) was generated with a formation

(13) Nofsinger, J. B.; Forest, S. E.; Simon, J. D. *J. Phys. Chem. B* **1999**, *103*, 11428–11432.
(14) Pezzella, A.; Panzella, L.; Crescenzi, O.; Napolitano, A.; Navaratnam, S.; Edge, R.; Land, E. J.; Barone, V.; d'Ischia, M. *J. Am. Chem. Soc.* **2006**, *128*, 15490–15498.
(15) (a) Zajac, G. W.; Gallas, J. M.; Cheng, J.; Eisner, M.; Moss, S. C.; Alvarada-Swaisgood, A. E. *Biochim. Biophys. Acta* **1994**, *1199*, 271–278. (b) Stark, K. B.; Gallas, J. M.; Zajac, G. W.; Golab, J. T.; Gidanian, S.; McIntire, T.; Farmer, P. J. *J. Phys. Chem. B* **2005**, *109*, 1970–1977.
(16) (a) Pezzella, A.; Napolitano, A.; d'Ischia, M.; Prota, G. *Tetrahedron* **1996**, *52*, 7913–7920. (b) Palumbo, P.; d'Ischia, M.; Crescenzi, O.; Prota, G. *Tetrahedron Lett.* **1987**, *28*, 467–470. (c) Palumbo, P.; d'Ischia, M.; Prota, G. *Tetrahedron* **1987**, *43*, 4203–4206.
(17) Pezzella, A.; Vogna, D.; Prota, G. *Tetrahedron* **2002**, *58*, 3681–3687.
(18) Pezzella, A.; Vogna, D.; Prota, G. *Tetrahedron: Asymmetry* **2003**, *14*, 1133–1140.
(19) Orlow, S. J.; Osber, M. E.; Pawelek, J. M. *Pigment Cell Res.* **1992**, *5*, 113–121.
(20) Tran, M. L.; Powell, B. J.; Meredith, P. *Biophys. J.* **2006**, *90*, 743–752.
(21) (a) Napolitano, A.; Di Donato, P.; Prota, G.; Land, E. J. *Free Radical Biol. Med.* **1999**, *27*, 521–528. (b) Land, E. J.; Ramsden, C. A.; Riley, P. A. *J. Photochem. Photobiol. B* **2001**, *64*, 123–135.
(22) Lambert, C.; Chacon, J. N.; Chedekel, M. R.; Land, E. J.; Riley, P. A.; Thompson, A.; Truscott, T. G. *Biochim. Biophys. Acta* **1989**, *993*, 12–20.

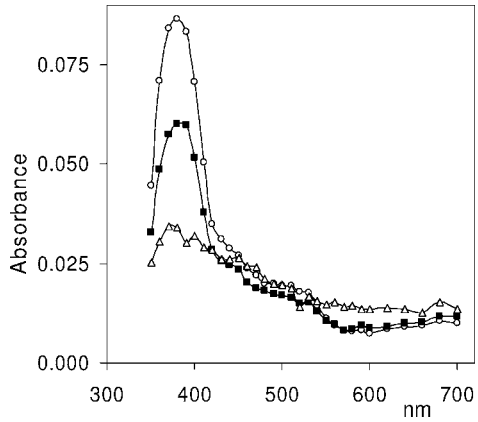

FIGURE 5. Changes in absorption at various times after pulse radiolysis of a N_2O-saturated solution of trimer **4** (1.5×10^{-4} M) in 0.5 M KBr/7.0×10^{-2} M phosphate buffer, pH 7.0: (○) 400 μs; (■) 2 ms; (Δ) 44 ms.

rate constant $k = 6.6 \times 10^8$ M^{-1} s^{-1} (for the reaction $Br_2^{-\bullet}$ + **4**) and decayed with second-order kinetics ($2k = 1.4 \times 10^8$ M^{-1} s^{-1}). Again, no significant chromophore generation above 400 nm was noted during semiquinone decay, though small inflections around 440 nm were apparent some milliseconds after the pulse. This behavior is similar to that of **1** and **3**. For all the compounds **2**−**4** after 44 ms, the absorptions eventually merged into a broad featureless band spanning over the visible region.

Overall, these experiments uncovered a number of significant, so far overlooked differences in the chromophoric species generated by oxidation of the oligomers from **1** and 5,6-dihydroxyindole, which can be summarized as follows. First, whereas semiquinone dimers from 5,6-dihydroxyindole exhibited intense bands in the 430−480 nm region,[14] semiquinone oligomers **2S**−**4S** displayed absorption bands in the same range and at markedly shorter wavelengths (360−370 nm). It is also noticeable that the absorption maxima of **2S**−**4S** are only slightly shifted relative to the monomer **1S** (maximum at 350 nm), in marked contrast with the large bathochromic shift observed on passing from the semiquinone monomer to the dimer in the 5,6-dihydroxyindole series.[14] Second, and most importantly, no significant chromophore in the visible region is produced from the decay of **2S**−**4S**, whereas the bimolecular decay of the semiquinone dimers from 5,6-dihydroxyindole resulted in intense visible absorption bands.[14] To inquire into the species generated by decay of semiquinone oligomers from **1**, and to find an explanation to the lack of visible chromophore generation, a theoretical investigation of the possible tautomeric forms of the two-electron oxidation products of dimers **2** and **3**, namely, **2Q** and **3Q**, was undertaken. The value of the quantum chemical approach for interpretation of pulse radiolysis data is underscored in recent work on transient semiquinones and quinones produced by oxidation of 5,6-dihydroxyindole derivatives.[14,23]

Theoretical Studies: Several rotamers can be envisaged for the *o*-quinone, quinone methide, and quinonimine tautomers of **2Q** and **3Q**, depending on the orientation of the indole rings around the interunit bond. To determine which of these structures may be a plausible candidate for the observed two-electron oxidation products of the dimers, all tautomeric quinones were geometry-optimized at the PBE0/6-31+G(d,p) level of theory,[24] using the polarizable continuum model (PCM)[25] to simulate the aqueous environment; the absorption spectra of all the energetically relevant species were computed using the time-dependent density functional theory (TDDFT)[26] approach (in aqueous solution), with the large 6-311++G(2d,2p) basis set.

For the purposes of the present study, the "hybrid" PBE0 functional was chosen, which has provided quite satisfactory energies and geometries for a wide range of organic and biological systems,[27] as well as a rather accurate description of low-lying excited states.[28] The performance of the selected DFT technique in predicting electronic absorption spectra of (dimeric) quinones has been specifically explored recently.[14]

The molecular structures of the main tautomers for **2Q** along with their relative energies are shown in Figure 6; a complete listing of the structures examined is presented in the Supporting Information.

DFT results suggest that localized quinones are the only significant tautomers in solution: with respect to the absolute minimum, extended forms are at least 4 kcal mol^{-1} less stable, while localized methide and quinonimine tautomers are even more disfavored. As far as the localized quinone form is concerned, the inter-ring dihedrals cluster with little oscillation around 115° for the *anti*-periplanar (*ap*) rotamers, while they span a larger interval for the *syn*-periplanar (*sp*) rotamers, with a value of 49° in the most stable form (**2Qm**). In this dimer series, alternative conformations differing only in the orientation of the OH groups of a dihydroxyindole ring (e.g., **2Qj**, **2Qk**, and **2Ql**) were separately optimized. However, "open" forms, such as **2Ql**, are invariably the least stable, while the other two forms, which feature a favorable intramolecular O−H···O interaction, are quite close in energy; therefore, in the following, open conformations were not considered, unless a preliminary inspection suggested that they could be involved in a different hydrogen bond pattern. In summary, the above calculations identified **2Qk**, **2Qm**, and **2Qn** as the primary determinants of the overall absorption properties of **2Q**, with slightly lower contributions from **2Qj** and **2Qo**.

Inclusion of harmonic vibrational contributions (see Supporting Information) entails a slightly larger separation between the more rigid extended quinone tautomers and the localized *o*-quinone forms but has a marginal impact on the overall

(23) Pezzella, A.; Crescenzi, O.; Natangelo, A.; Panzella, L.; Napolitano, A.; Navaratnam, S.; Edge, R.; Land, E. J.; Barone, V.; d'Ischia, M. *J. Org. Chem.* **2007**, *72*, 1595–1603.

(24) Adamo, C.; Barone, V. *J. Chem. Phys.* **1999**, *110*, 6158–6170.

(25) (a) Miertus, S.; Scrocco, E.; Tomasi, J. *Chem. Phys.* **1981**, *55*, 117–129. (b) Cossi, M.; Scalmani, G.; Rega, N.; Barone, V. *J. Chem. Phys.* **2002**, *117*, 43–54. (c) Scalmani, G.; Barone, V.; Kudin, K. N.; Pomelli, C. S.; Scuseria, G. E.; Frisch, M. J. *Theor. Chem. Acc.* **2004**, *111*, 90–100. (d) Tomasi, J.; Mennucci, B.; Cammi, R. *Chem. Rev.* **2005**, *105*, 2999–3093.

(26) (a) Stratmann, R. E.; Scuseria, G. E.; Frisch, M. J. *J. Chem. Phys.* **1998**, *109*, 8218–8224. (b) Bauernschmitt, R.; Ahlrichs, R. *Chem. Phys. Lett.* **1996**, *256*, 454–464. (c) Casida, M. E.; Jamorski, C.; Casida, K. C.; Salahub, D. R. *J. Chem. Phys.* **1998**, *108*, 4439–4449. (d) Adamo, C.; Scuseria, G. E.; Barone, V. *J. Chem. Phys.* **1999**, *111*, 2889–2899.

(27) (a) Improta, R.; Barone, V. *J. Am. Chem. Soc.* **2004**, *126*, 14320–14321. (b) Benzi, C.; Improta, R.; Scalmani, G.; Barone, V. *J. Comput. Chem.* **2002**, *23*, 341–350. (c) Langella, E.; Rega, N.; Improta, R.; Crescenzi, O.; Barone, V. *J. Comput. Chem.* **2002**, *23*, 650–661. (d) Improta, R.; Mele, F.; Crescenzi, O.; Benzi, C.; Barone, V. *J. Am. Chem. Soc.* **2002**, *124*, 7857–7865. (e) Improta, R.; Barone, V.; Rega, N. *Acc. Chem. Res.* **2008**, *41*, 605–616.

(28) (a) Jacquemin, D.; Wathelet, V.; Perpete, E. A. *J. Phys. Chem. A* **2006**, *110*, 9145–9152. (b) Preat, J.; Jacquemin, D.; Wathelet, V.; Andre, J.-M.; Perpete, E. A. *J. Phys. Chem. A* **2006**, *110*, 8144–8150. (c) Jacquemin, D.; Preat, J.; Wathelet, V.; Fontaine, M.; Perpete, E. A. *J. Am. Chem. Soc.* **2006**, *128*, 2072–2083. (d) Crescenzi, O.; Pavone, M.; De Angelis, F.; Barone, V. *J. Phys. Chem. B* **2005**, *109*, 445–453. (e) Aquilante, F.; Cossi, M.; Crescenzi, O.; Scalmani, G.; Barone, V. *Mol. Phys.* **2003**, *101*, 1945–1953. (f) Adamo, C.; Barone, V. *Chem. Phys. Lett.* **2000**, *330*, 152–160.

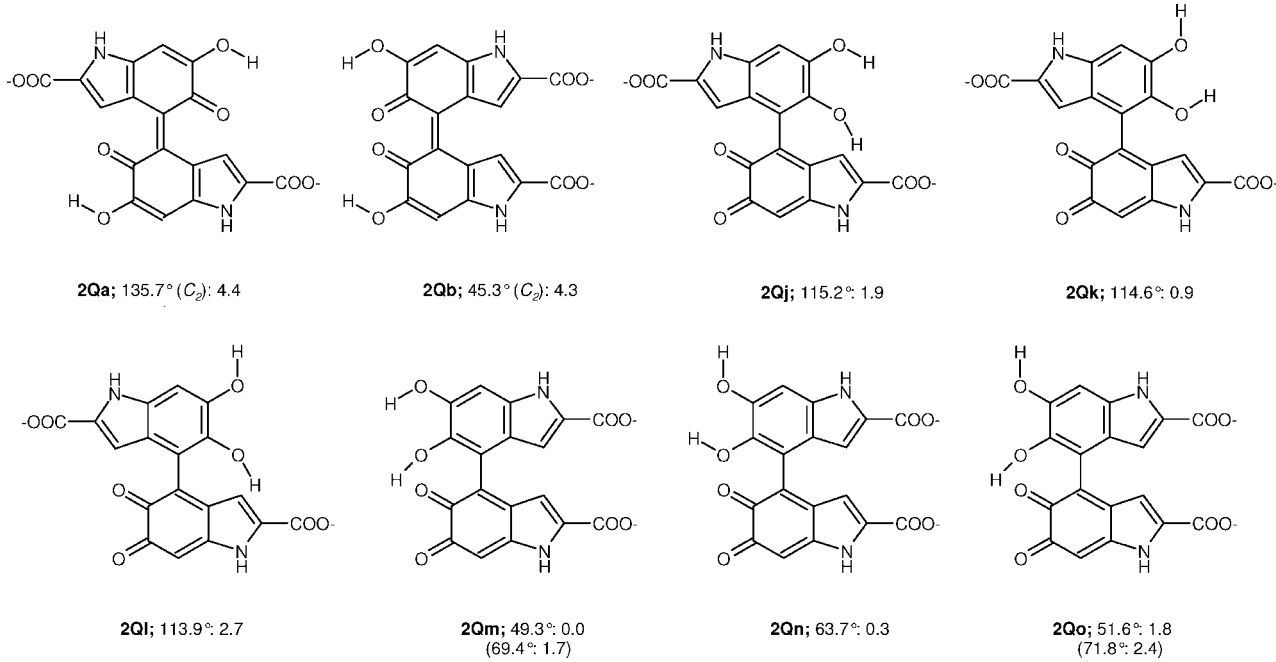

FIGURE 6. Structures and relative energies (kcal mol^{-1}) of several tautomers/conformers of **2Q**, computed at the PBE0/6-31+G(d,p) level in aqueous solution (PCM). The inter-ring C5−C4−C4′−C5′ dihedral (degrees) (and for symmetric structures, the point group) is reported. Entries in parentheses refer to alternative conformers.

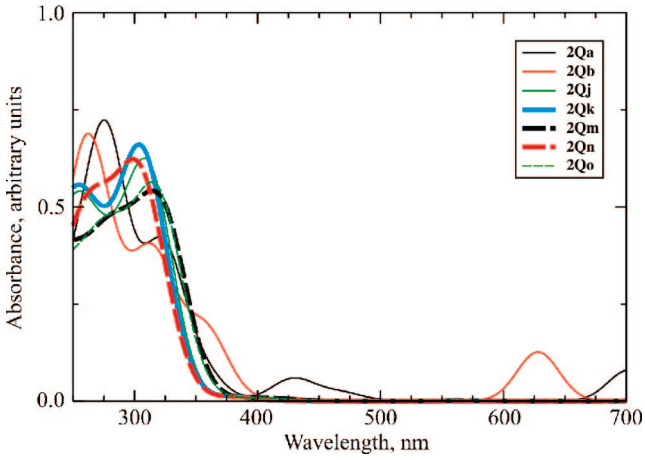

FIGURE 7. UV−vis spectra of several tautomers/conformers of **2Q**, computed at the PBE0/6-311++G(2d,2p)//PBE0/6-31+G(d,p) level in aqueous solution (PCM). The traces of the most stable forms are highlighted in bold.

picture. As a further check, single point energies were also computed at the MP2/6-31+G(d,p)/PCM level for all structures: while a general flattening of the potential energy surface is observed, this effect is not marked enough as to significantly alter the predictions obtained at the DFT level. Computed absorption spectra of all significant tautomers/conformers are given in Figure 7: the extended quinone forms **2Qa** and **2Qb** are also included for comparison purposes.

As far as the *o*-quinone forms are concerned, the computed absorption maxima are all quite close, with a double band at ca. 260 and 305 nm, but no significant absorption in the visible, a prediction which agrees with the experimentally measured spectrum of the species formed by second-order decay of the transient **2S**.

With respect to **2Q**, the unsymmetrical structure of **3Q** implies a larger number of possible tautomers/conformers. A complete exploration at the usual PBE0/6-31+G(d,p)/PCM level (see Supporting Information) allowed us to identify localized quinone tautomers as the most stable structures (Figure 8), with 4-substituted and 7-substituted quinones displaying similar stabilities.

Inter-ring dihedrals also showed a close correspondence between the two series, spanning the range 47−64 and 112−119° for *sp* and *ap* rotamers, respectively; the smaller dihedrals can usually be traced back to the formation of an inter-ring O−H···O hydrogen bond. As in the case of **2Q**, localized methide and quinonimine tautomers are always strongly disfavored; however, the extended tautomer **3Qa** is only 1.8 kcal mol^{-1} higher in energy with respect to the absolute minimum (**3Qq**); an intersubunit hydrogen bond involving the indole NH group and the adjacent carbonyl oxygen atom probably contributes to the enhanced stability of **3Qa**; as a matter of fact, the corresponding *Z* structure **3Qb** lies 2.6 kcal mol^{-1} higher in energy. It is interesting to note that at the MP2/PCM level (see Supporting Information) the extended forms shift to even lower relative energies (**3Qa** at 0.3 kcal mol^{-1} from the minimum, which in this case is **3Qm**); by contrast, harmonic vibrational corrections tend to increase significantly this separation. The computed absorption spectra of various forms of **3Q** are given in Figure 9. All localized quinone tautomers feature strong bands around 250 and 310 nm but only very weak absorptions in the visible region; however, for the highly delocalized structure **3Qa**, relatively strong bands at 450 and 640 nm are predicted. It would be tempting to associate these computed maxima to the modest peaks at 440 (sh) and 620 nm observed in the pulse radiolysis oxidation of **3**; however, the timing of their appearance does not support this hypothesis.

Since it is known that the PCM model can show limitations in the accurate description of highly specific solute−solvent interactions, the computed UV−vis spectrum of **2Qm** was used as a test case to evaluate the results of a cluster/PCM approach, which has proved very versatile in reproducing static and

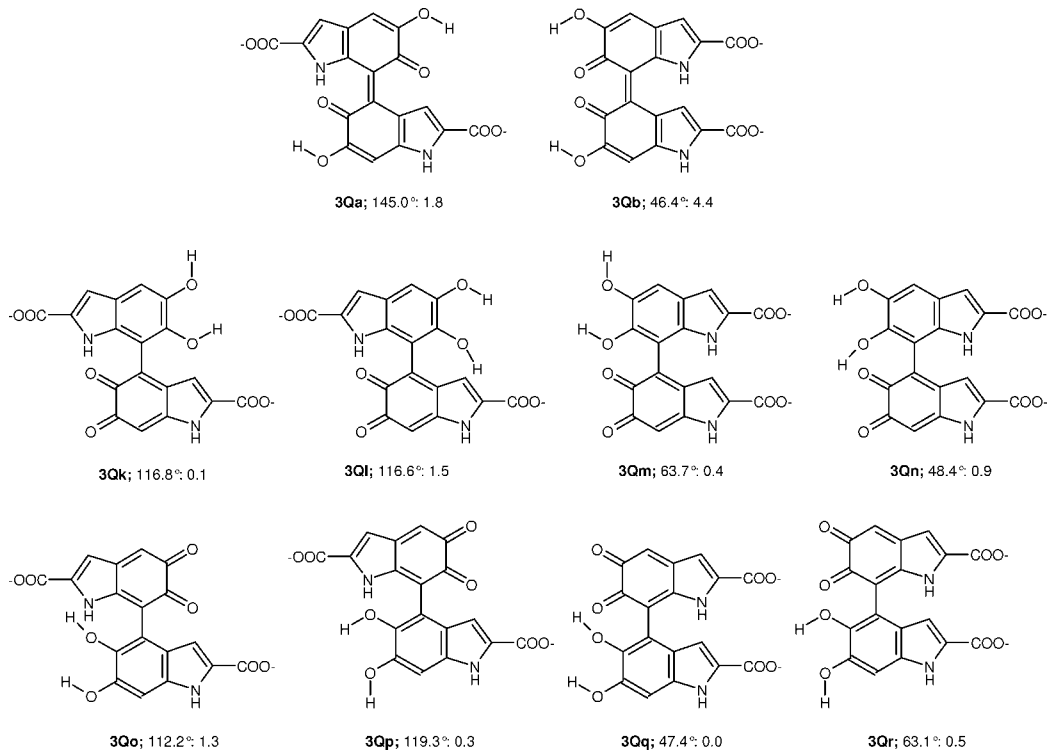

FIGURE 8. Structures and relative energies (kcal mol^{-1}) of several tautomers/conformers of **3Q**, computed at the PBE0/6-31+G(d,p) level in aqueous solution (PCM). The inter-ring C5−C4−C7′−C6′ dihedral (degrees) is reported.

dynamic solvation effects.[28d,29] Thus, TDDFT/PCM computations were performed on some water adducts of **2Qm**, in which an explicit water molecule was hydrogen bonded to a carboxyl, carbonyl, or hydroxyl group. However, in the wavelength region of interest (above ca. 300 nm), the computed spectral traces turned out to be almost unchanged with respect to those computed with PCM alone (see Supporting Information). Such insensitivity to the details of the hydrogen bonding geometry is probably related to the nature of the dominant transitions that involve mainly delocalized π orbitals. Thus, for example, the principal transitions in the computed UV spectrum of **3Qk** and **3Ql** are at 324/323 nm ($f = 0.17/0.19$), 307/307 ($f = 0.18/0.14$), and 301/305 nm ($f = 0.22/0.22$), respectively. The first transition to the LUMO involves π orbitals essentially localized on the quinone moiety: as a matter of fact, a closely similar excitation can be identified in the computed spectrum of the 5,6-indolequinone-2-carboxylate (323 nm, $f = 0.16$, at this theory level). The transition at 307 nm (HOMO → LUMO+1) has a more marked charge transfer character in that the HOMO is mostly localized on the catechol ring, whereas the LUMO+1 is strongly delocalized across the biindolyl system. Finally, the last transition is HOMO-1 → LUMO+1 in character, and again, the HOMO-1 has the highest coefficients on the catecholic ring. Apart from quantitative differences, the situation is reproduced in the *syn*-periplanar counterparts (i.e., **3Qm** and **3Qn**). The computed spectra of the 7-substituted quinone series are slightly more complex. The main features are still attributable to the set of three transitions discussed above, of which the HOMO → LUMO+1 is now predominant; however, some longer wavelength transitions appear with enhanced intensity (**3Qo**: 357 nm, $f = 0.03$; **3Qp**: 353 nm, $f = 0.07$; **3Qq**: 363 nm, $f = 0.04$, and 335 nm, $f = 0.05$; **3Qr**: 341 nm, $f = 0.07$). These can be described in terms of promotions from a mixture of orbitals spanning both rings to the LUMO, which is still well localized on the quinone moiety. As to the spectrum of the extended form **3Qa**, the 640 nm transition ($f = 0.115$) is essentially HOMO-2 → LUMO in character; the 450 nm band results from the overlap of several transition, of which the principal one (451 nm, $f = 0.043$) displays a (much less clear) HOMO-6 → LUMO character. A comparison of orbitals crucially involved in originating the UV−vis spectrum for **3Qk** (representative of the 4-substituted quinone series), **3Qq** (for the 7-substituted quinone series), and **3Qa** (the most stable of the two extended tautomers) is provided in the Supporting Information.

The body of calculations described above provides a consistent picture of the quinones from dimers **2** and **3** that highlighted localized 5,6-indolequinone−dihydroxyindole structures as the most stable tautomers. These exhibit expected absorption properties that are consistent with the failure to detect intensely absorbing species in the visible region. On the basis of computed absorption spectra, the appearance of weak transient absorptions around 440 nm by bimolecular decay of **3S** (Figure 4) cannot be safely attributed to any of the stable *o*-quinone tautomers of **3Q**. While it is possible that a non-negligible proportion of extended quinone tautomers is in equilibrium with the dominant localized quinone tautomers of **3Q**, alternative explanations can be considered, involving, for example, the formation of free radical coupling products of semiquinone **3S**, with poorly predictable absorption properties. This however cannot be assessed based on available data. Similar arguments can be confidently used to explain the unexpectedly modest absorption changes accompanying oxidation of the trimer **4**, although a

(29) (a) Barone, V.; Crescenzi, O.; Improta, R. *Quant. Struct.-Act. Relat.* **2002**, *21*, 105–118. (b) Cossi, M.; Crescenzi, O. *J. Chem. Phys.* **2003**, *118*, 8863–8872. (c) Pavone, M.; Benzi, C.; De Angelis, F.; Barone, V. *Chem. Phys. Lett.* **2004**, *395*, 120–126. (d) Ciofini, I.; Adamo, C.; Barone, V. *J. Chem. Phys.* **2004**, *121*, 6710–6718.

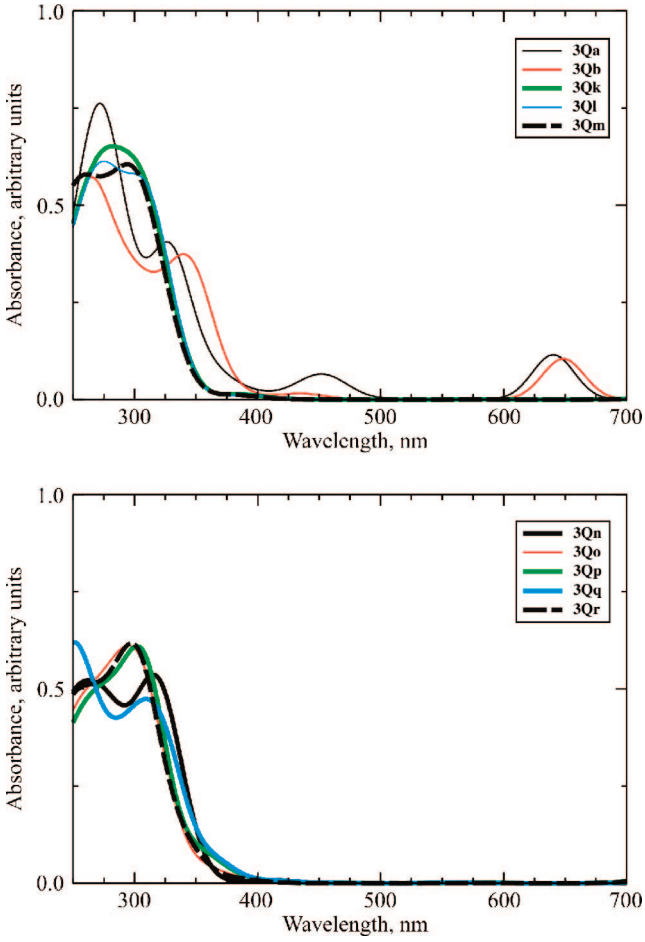

FIGURE 9. UV−vis spectra of significant tautomers/conformers of **3Q**, computed at the PBE0/6-311++G(2d,2p)//PBE0/6-31+G(d,p) level in aqueous solution (PCM). The traces of the most stable forms are highlighted in bold.

satisfactory computational investigation of this compound proved too demanding for the DFT approach used.

The double peak at 350−380 nm in the spectrum of the semiquinone transients from dimer **2** (Figure 3) may be due either to transitions from/to distinct electronic levels or to a vibronic feature, but this was not investigated at a computational level. In this regard, the contribution of different tautomers or conformers to the absorption maximum cannot be ruled out.

Conclusions

We have used an integrated pulse radiolysis and DFT approach to demonstrate for the first time that the short-lived species produced by pulse radiolysis oxidation of three representative oligomers from **1** lack significant absorption bands in the visible region (400−700 nm) due to their tendency to adopt twisted conformations with significant dihedral angles. These results complement and expand those of a previous study on 5,6-dihydroxyindole dimers[14] and would now allow us to provide a convincing explanation of the different absorption properties and visual colorations of eumelanin-like polymers from 5,6-dihydroxyindole and from **1**. The key concept that underpins this difference relates to the impact of hindered rotation around inter-ring bonds on the effective conjugation length in eumelanin-like polymers from **1**[20] and the consequent assumption of spiral staircase-like scaffolds for their main structural components with multiple breaks of π-electron conjugation. Why eumelanin from **1**, though paler than that from 5,6-dihydroxyindole, is still dark-brown in color cannot be explained based on the present results. Diverse factors that concur to eumelanin optical properties need to be clarified, for example, the fate of the two-electron oxidation products around 400−550 nm and the role of extended forms such as **3Qa**, and are the focus of ongoing work. A relevant point in this connection is whether the system polymerizes or rather stable oligomeric species are formed. A high degree of oligomerization leading to a final end point stabilization, given the lack of further spectral changes, seems the answer, but this requires confirmation.

The relevance of these results to natural eumelanins remains also to be assessed since the anaerobic pulse radiolysis conditions of this study may differ significantly from those expected within biological environments, where other reactions may become important. However, the new information gained from this study may pave the way to novel important advances in the elucidation of eumelanin optical properties and may guide the design of new bioinspired materials for potential application in optoelectronics.

Experimental Section

5,6-Dihydroxyindole-2-carboxylic acid (**1**)[30] and the acetyl derivatives of dimers **2** and **3** and trimer **4**[17,18] were prepared as previously reported.

Pulse Radiolysis: The pulse radiolysis experiments were performed with the 12 MeV linear accelerator at the Daresbury Laboratory, using the Free Radical Research Facility.[31] This accelerator provides pulse lengths of between 0.2 and 2 μs with doses up to 30 Gy using quartz capillary cells of optical path 2.5 cm. Absorbed doses were determined from the transient $(CNS)_2^{\bullet-}$ formation in air-saturated potassium thiocyanate solutions (10 mM) using a G of 0.30 μM/Gy and ε (500 nm) = 7100 M^{-1} cm^{-1}.[32] The estimates of the molar absorption coefficients and rate constants are considered to be correct to ±15%. In a typical experiment, a solution of the appropriate indole as acetyl derivative in methanol (15 mM) was treated under a N_2O atmosphere with a solution of 0.025 M trisodium phosphate containing 0.5 M KBr up to a 0.15 mM concentration, and after 1 min, the pH of the solution was taken to 7.0 by addition of NaH_2PO_4 (0.07 M final concentration of phosphate buffer). The resulting mixture was subjected to pulse radiolysis.

Computational Methods: All calculations were performed with the Gaussian package of programs.[33] Geometries were optimized at the DFT level of theory using the PBE0 functional with the 6-31+G(d,p) basis set.[34] The PBE0 (also referred to as PBE1PBE) is a hybrid functional obtained by combining a predetermined amount of exact exchange with the Perdew−Burke−Ernzerhof exchange and correlation functionals.[24] To simulate the aqueous environment, the polarizable continuum model (PCM)[25] was used. In view of the faster convergence, a scaled van der Waals cavity based on universal force field (UFF) radii[35] was used, and polarization charges were modeled by spherical Gaussian func-

(30) Edge, R.; d'Ischia, M.; Land, E. J.; Napolitano, A.; Navaratnam, S.; Panzella, L.; Pezzella, A.; Ramsden, C. A.; Riley, P. A. *Pigment Cell Res.* **2006**, *19*, 443–450.

(31) (a) Butler, J.; Hodgson, B. W.; Hoey, B. M.; Land, E. J.; Lea, J. S.; Lindley, E. J.; Rushton, F. A. P.; Swallow, A. J. *Radiat. Phys. Chem.* **1989**, *34*, 633–646. (b) Holder, D. J.; Allan, D.; Land, E. J.; Navaratnam, S. In *Proceedings of the 8th European Particle Accelerator Conference*; Garvey, T., Le Duff, J., Le Roux, P., Petit-Jean-Genaz, C., Poole, J., Rivki, L., Eds.; European Physical Society: Paris, 2002; pp 2804−2806.

(32) (a) Buxton, G. V.; Stuart, C. R. *J. Chem. Soc., Faraday Trans.* **1995**, *91*, 279–281. (b) Adams, G. E.; Boag, J. W.; Currant, J.; Michael, B. D. In *Pulse Radiolysis*; Ebert, M., Keene, J. P., Swallow, A. J., Baxendale, J. H., Eds.; Academic Press: London, 1965; pp 117−129.

tions;[36] however, the final computation of PCM energies relies on the highly optimized and widely tested UAHF radii.[37] Significant minima were checked by computing the harmonic vibrational frequencies. MP2/PCM single point energies were computed with the same basis set for comparison purposes. Electronic absorption spectra of significant tautomers were estimated on the basis of excitation energy calculations using the TDDFT approach.[26] The PBE0 functional with the large 6-311++G(2d,2p) basis set was used for TDDFT computations. In this case, the linear response nonequilibrium PCM model was used.[38] To produce graphs of computed UV−vis spectra, transitions above 190 nm were selected, and an arbitrary Gaussian line width of 20 nm was imposed.

Acknowledgment. This paper is dedicated to the memory of Professor R. A. Nicolaus (1920−2008) who pioneered studies of melanin chemistry at Naples. This work was supported by grants from Italian MIUR-PRIN 2006. L.P. is thankful to "L'ORÉAL Italia Per le Donne e la Scienza" for a research fellowship. All computations were performed on the large-scale computer facilities of the VILLAGE network (http://village.unina.it). The pulse radiolysis experiments were carried out at the Free Radical Research Facility (Station 0.1) in the Synchrotron Radiation Department of the STFC Daresbury Laboratory, Warrington, U.K. and were financially supported by the EC Grant No. AP46154. We thank the "Centro Interdipartimentale di Metodologie Chimico-Fisiche" (CIMCF, University of Naples Federico II) for NMR and mass spectrometry facilities.

Supporting Information Available: Structures and relative energies of tautomers/conformers of **2Q** and **3Q** computed at the PBE0/6-31+G(d,p) level in aqueous solution (PCM), coordinates of tautomers/conformers of **2Q** and **3Q**, relative energies of selected tautomers/conformers of **2Q** and **3Q** computed at the MP2/6-31+G(d,p) level in aqueous solution (PCM), relative free energies of selected tautomers/conformers of **2Q** and **3Q** computed at the PBE0/6-31+G(d,p) level in aqueous solution (PCM) with inclusion of harmonic vibrational contributions, transition wavelengths and oscillator strengths computed at the PBE0/6-311+G(2d,2p)/PCM//PBE0/6-31+G(d,p)/PCM level for **2Qm**, kinetics of pulse radiolytic oxidation of compounds **2**−**4** at different wavelengths, changes in absorption at various times after pulse radiolysis of **3**, isodensity surfaces of selected molecular orbitals of **3Qk**, **3Qq**, and **3Qa** computed at the PBE0/6-311++G(2d,2p)//PBE0/6-31+G(d,p) level in aqueous solution (PCM). This material is available free of charge via the Internet at http://pubs.acs.org.

JO900250V

(33) (a) Frisch, M. J. ; Trucks, G. W.; Schlegel, H. B.; Scuseria, G. E.; Robb, M. A.; Cheeseman, J. R.; Montgomery, J. A., Jr.; Vreven, T.; Kudin, K. N.; Burant, J. C.; Millam, J. M.; Iyengar, S. S.; Tomasi, J.; Barone, V.; Mennucci, B.; Cossi, M.; Scalmani, G.; Rega, N.; Petersson, G. A.; Nakatsuji, H.; Hada, M.; Ehara, M.; Toyota, K.; Fukuda, R.; Hasegawa, J.; Ishida, M.; Nakajima, T.; Honda, Y.; Kitao, O.; Nakai, H.; Klene, M.; Li, X.; Knox, J. E.; Hratchian, H. P.; Cross, J. B.; Bakken, V.; Adamo, C.; Jaramillo, J.; Gomperts, R.; Stratmann, R. E.; Yazyev, O.; Austin, A. J.; Cammi, R.; Pomelli, C.; Ochterski, J. W.; Ayala, P. Y.; Morokuma, K.; Voth, G. A.; Salvador, P.; Dannenberg, J. J.; Zakrzewski, V. G.; Dapprich, S.; Daniels, A. D.; Strain, M. C.; Farkas, O.; Malick, D. K.; Rabuck, A. D.; Raghavachari, K.; Foresman, J. B.; Ortiz, J. V.; Cui, Q.; Baboul, A. G.; Clifford, S.; Cioslowski, J.; Stefanov, B. B.; Liu, G.; Liashenko, A.; Piskorz, P.; Komaromi, I.; Martin, R. L.; Fox, D. J.; Keith, T.; Al-Laham, M. A.; Peng, C. Y.; Nanayakkara, A.; Challacombe, M.; Gill, P. M. W.; Johnson, B.; Chen, W.; Wong, M. W.; Gonzalez, C.; Pople, J. A. *Gaussian 03*, revision C.02; Gaussian, Inc.: Wallingford, CT, 2004. (b) Frisch, M. J. ; Trucks, G. W.; Schlegel, H. B.; Scuseria, G. E.; Robb, M. A.; Cheeseman, J. R.; Montgomery, J. A., Jr.; Vreven, T.; Scalmani, G.; Kudin, K. N.; Iyengar, S. S.; Tomasi, J.; Barone, V.; Mennucci, B.; Cossi, M.; Rega, N.; Petersson, G. A.; Nakatsuji, H.; Hada, M.; Ehara, M.; Toyota, K.; Fukuda, R.; Hasegawa, J.; Ishida, M.; Nakajima, T.; Honda, Y.; Kitao, O.; Nakai, H.; Li, X.; Hratchian, H. P., Peralta, J. E.; Izmaylov, A. F.; Heyd, J. J.; Brothers, E.; Staroverov, V.; Zheng, G.; Kobayashi, R.; Normand, J.; Burant, J. C.; Millam, J. M.; Klene, M.; Knox, J. E.; Cross, J. B.; Bakken, V.; Adamo, C.; Jaramillo, J.; Gomperts, R.; Stratmann, R. E.; Yazyev, O.; Austin, A. J.; Cammi, R.; Pomelli, C.; Ochterski, J. W.; Ayala, P. Y.; Morokuma, K.; Voth, G. A.; Salvador, P.; Dannenberg, J. J.; Zakrzewski, V. G.; Dapprich, S.; Daniels, A. D.; Strain, M. C.; Farkas, O.; Malick, D. K.; Rabuck, A. D.; Raghavachari, K.; Foresman, J. B.; Ortiz, J. V.; Cui, Q.; Baboul, A. G.; Clifford, S.; Cioslowski, J.; Stefanov, B. B.; Liu, G.; Liashenko, A.; Piskorz, P.; Komaromi, I.; Martin, R. L.; Fox, D. J.; Keith, T.; Al-Laham, M. A.; Peng, C. Y.; Nanayakkara, A.; Challacombe, M.; Chen, W.; Wong, M. W.; Pople, J. A. *Gaussian Development Version*, revision F.01; Gaussian, Inc.: Wallingford, CT, 2006.

(34) (a) Francl, M. M.; Petro, W. J.; Hehre, W. J. S.; Binkley, J.; Gordon, M. S.; DeFrees, D. J.; Pople, J. A. *J. Chem. Phys.* **1982**, *77*, 3654–3665. For a general introduction to basis sets, see: (b) Foresman, J. B.; Frisch, A. *Exploring Chemistry with Electronic Structure Methods*, 2nd ed.; Gaussian, Inc.: Pittsburgh, PA, 1996.

(35) Rappé, A. K.; Casewit, C. J.; Colwell, K. S.; Goddard, W. A., III.; Skiff, W. M. *J. Am. Chem. Soc.* **1992**, *114*, 10024–10035.

(36) (a) York, D. A.; Karplus, M. *J. Phys. Chem. A* **1999**, *103*, 11060–11079. (b) Caricato, M.; Scalmani, G.; Frisch, M. J. In *Continuum Solvation Models in Chemical Physics*; Mennucci, B., Cammi, R., Eds.; John Wiley & Sons: Chichester, 2007; pp 64−81.

(37) Barone, V.; Cossi, M.; Tomasi, J. *J. Chem. Phys.* **1997**, *107*, 3210–3221.

(38) Cossi, M.; Barone, V. *J. Phys. Chem. A* **2000**, *104*, 10614–10622.